NANO LETTERS

Letter

pubs.acs.org/NanoLett

Coulomb Oscillations in a Gate-Controlled Few-Layer Graphene Quantum Dot

Yipu Song,[*,†] Haonan Xiong,[†,‡] Wentao Jiang,[†,‡] Hongyi Zhang,[†] Xiao Xue,[†] Cheng Ma,[†] Yulin Ma,[†] Luyan Sun,[†] Haiyan Wang,[†] and Luming Duan[*,†,§]

[†]Center for Quantum Information, IIIS, Tsinghua University, Beijing 100084, China

[‡]Department of Physics, Tsinghua University, Beijing 100084, China

[§]Department of Physics, University of Michigan, Ann Arbor, Michigan 48109, United States

Supporting Information

ABSTRACT: Graphene quantum dots could be an ideal host for spin qubits and thus have been extensively investigated based on graphene nanoribbons and etched nanostructures; however, edge and substrate-induced disorders severely limit device functionality. Here, we report the confinement of quantum dots in few-layer graphene with tunable barriers, defined by local strain and electrostatic gating. Transport measurements unambiguously reveal that confinement barriers are formed by inducing a band gap via the electrostatic gating together with local strain induced constriction. Numerical simulations according to the local top-gate geometry confirm the band gap opening by a perpendicular electric field. We investigate the magnetic field dependence of the energy-level spectra in these graphene quantum dots. Experimental results reveal a complex evolution of Coulomb oscillations with the magnetic field, featuring kinks at level crossings. The simulation of energy spectrum shows that the kink features and the magnetic field dependence are consistent with experimental observations, implying the hybridized nature of energy-level spectrum of these graphene quantum dots.

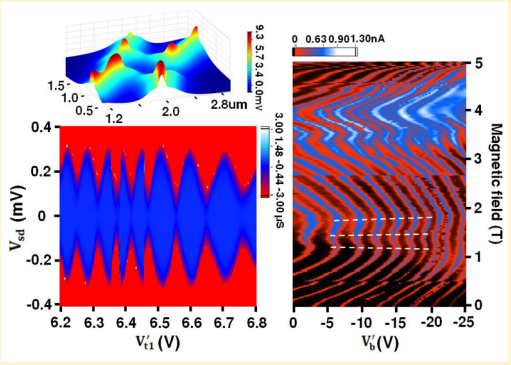

KEYWORDS: *Few-layer graphene, quantum dot, Landau levels, Coulomb oscillation, tunable barriers*

Graphene has received tremendous attention as a promising candidate for nanoelectronics and quantum computing owing to its extraordinary electronic properties.[1,2] Quantum dots (QDs) confined in graphene could be an ideal host for spin qubits. A long coherence time up to 80 μs has been theoretically predicted in graphene QDs due to the weak spin−orbit coupling and hyperfine interaction,[3] which is 4 orders of magnitude of the predicted 5 ns for GaAs in the absence of nuclear-spin polarization.[4] To define spin qubits in graphene, a band gap has to be opened up to create a tunable QD. Hence the modification of graphene structures for opening its band gap is a crucial step toward practical applications. Graphene QDs have been extensively investigated based on graphene nanoribbons and etched nanostructures; however, edge and substrate-induced disorders severely limit device functionality.[5−7]

Few-layer graphene (FLG) is the only known material to exhibit an electric field- and stacking-dependent band structure.[8−10] Stacking order in FLG provides an important yet rarely explored degree of freedom for tuning its electronic properties. For instance, by breaking the layer inversion symmetry in AB-stacked bilayer graphene, an external perpendicular electric field can open an energy gap by local electrostatic gating.[11,12] Gate-defined QDs have been demonstrated in suspended bilayer graphene.[11] Compared with monolayer and bilayer graphene, trilayer graphene has more complex interlayer interactions resulting in richer electronic structure.[10] ABC-stacked trilayer graphene (r-TLG) is predicted to be semiconducting with a tunable band gap.[8−10] However, confining quantum dots has not been achieved yet in TLG. A perpendicular magnetic field breaks the time-reversal symmetry in graphene and thus lifts the valley degeneracy.[14] That is crucial to perform two-qubit gates using Heisenberg exchange coupling of electron spins in graphene QDs.[15] In this Letter, we report an experimental approach to define QDs in FLG with tunable barriers and demonstrate a hybridized nature of energy-level spectrum of QD, featuring kinks at level crossings in the presence of a perpendicular magnetic field.

We investigated the application of nanoscale top gates on exfoliated graphene to define QD devices. The device fabrication involves multiple e-beam lithography processes to make source−drain contacts and local top gates. Graphene flakes were exfoliated onto highly doped Si substrates terminated by 300 nm SiO_2. The flake thickness and stacking

Received: June 20, 2016
Revised: September 9, 2016

DOI: 10.1021/acs.nanolett.6b02522
Nano Lett. XXXX, XXX, XXX−XXX

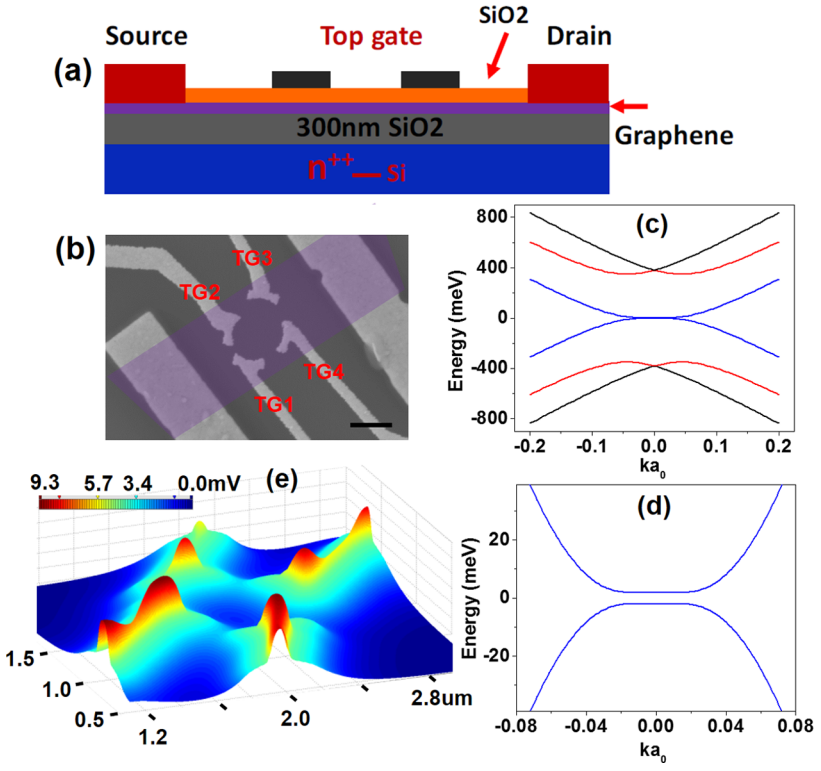

Figure 1. (a) Schematic cross-section of a graphene QD device. (b) SEM image of a measured r-TLG QD device D1. The scale bar is 500 nm. The graphene sheet is highlighted in purple. (c) Low-energy band structure of r-TLG around the K point in the region beneath the top gate, upon electrical gating $V_t' = 5.0$ V and $V_b' = -22.6$ V. (d) Close-up of (c) showing a band gap of 4.0 meV. (e) A simulated profile of barrier potential for the QD device shown in b upon electrical gating $V_t' = 5.0$ V and $V_b' = -22.6$ V.

order were characterized by a combination of optical contrast,[16] AFM and Raman spectroscopy (see Supporting Information).[17−19] Selected FLG (bilayer or trilayer) flakes were located relative to pre-existing fiducial markers. Ti/Au (10 nm/80 nm) source−drain metal contacts were deposited by ebeam evaporation. Samples were annealed at 350 °C for 3 h to remove PMMA residues from the graphene surface, followed by 100 nm SiO_2 deposition by plasma-enhanced chemical vapor deposition (PECVD). Top gates were patterned with e-beam lithography followed by e-beam evaporation of metal films Ti/Au (10 nm/60 nm). The device structure is shown schematically in Figure 1a, and a SEM image of a typical QD device is shown in Figure 1b. After fabrication, the device chip was wire-bonded and loaded onto the mix chamber of a dilution refrigerator. Transport measurements were carried out at a base temperature about 10 mK unless otherwise mentioned. RC, π, and copper powder filters in the measurement circuit were used to filter out measurement noise. Upon applying a DC source−drain voltage V_{sd}, the device current I_{sd} was measured using a current−voltage preamplifier at a noise floor of 0.5 pA/$\sqrt{\text{Hz}}$. A voltage V_b' applied to the degenerately doped Si substrate provided a global back gate.

Eleven FLG QD devices and 16 field-electron-transistor (FET) devices have been investigated to varying levels of detail at a low temperature. At room temperature, all devices show a linear $I_{sd}-V_{sd}$ behavior indicating a resistance in range of 1−27 kΩ with the back and top gate voltages all zero, as shown by solid curves in Figure 2a for four representative QD devices (D1−D4) and two FET devices (D5, D6). The detailed description of measured devices is shown in Table S1 in the Supporting Information. Suppression of device conductance to varying degrees has been observed as the temperature is lowered for eight QD devices from 11 ones. A nonlinear characteristic of $I_{sd}-V_{sd}$ was usually found for QD devices at a base temperature of 10 mK, as shown in Figure 2b for QD device D1−D4. This conductance suppression is consistent with the observation in the recent experimental and theoretical studies.[13,20,21] It is likely to be caused by strain due to a mismatch in thermal expansion coefficients of gate metal, insulating layer, and substrate.[13] This hypothesis is supported by the nonsuppression of conductance for graphene FET devices without top gates. Although the device conductance varies, $I_{sd}-V_{sd}$ curves keep linear for 16 FET devices measured as the temperature decreases to the base temperature, as shown as dashed lines in Figure 2a for two representative FET devices (D5 and D6). The local strain could be stronger in smaller top gate structures with the same dielectric layer thickness. The enhanced conductance suppression observed in QD devices, confined by smaller top gates with a dot size less than 100 nm, further confirms the hypothesis that the local strain plays a crucial role for top-gated graphene QD devices. For eight FLG QD devices, the conductance is suppressed but not completely pinched off at the base temperature. By applying a perpendicular electrical field through the back gate and top gates, tunnel barriers are further enhanced beneath the top gates, eventually leading to a pinch-off to define a dot constriction. Figure 2c shows low-bias conductance measurements ($V_{sd} = 0.5$ mV) for the device D1 as varying gate-voltage configurations at a base temperature. With the back and top gate voltages all zero, the device conductance is significantly reduced to 0.270 e^2/h at 10 mK. Under the individual top-gate voltage sweeping from 0 to 10 V, the device conductance can

DOI: 10.1021/acs.nanolett.6b02522
Nano Lett. XXXX, XXX, XXX−XXX

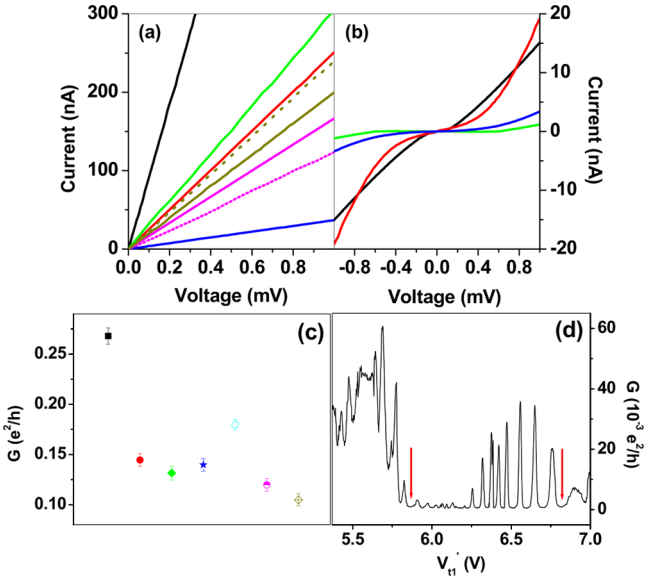

Figure 2. (a) I_{sd}−V_{sd} characteristics for the QD device D1 (black), D2 (red), D3 (blue), and D4 (green) at room temperature. I_{sd}−V_{sd} curves for the FET device D5 (magenta) and D6 (dark yellow) at room temperature (solid line) and a base temperature of 10 mK (dashed line), respectively. (b) Nonlinear characteristics of I_{sd}−V_{sd} for the QD device D1 (black), D2 (red), D3 (blue), and D4 (green) at 10 mK. The back and top gate voltages are all held zero. (c) Minimum conductance (V_{sd} = 0.5 mV) for device D1 as varying gate-voltage configurations (V'_b, V'_{t1}, V'_{t2}, V'_{t3}, and V'_{t4}) at a base temperature. Error bars indicate the uncertainty of conductance measurements. ■ (black): (0 V, 0 V, 0 V, 0 V, 0 V); ● (red): (0 V, 4.0 V, 0 V, 0 V, 0 V); ◆ (green): (0 V, 0 V, 4.6 V, 0 V, 0 V); ★ (blue): (0 V, 0 V, 0 V, 2.4 V, 0 V); ○ (cyan): (0 V, 0 V, 0 V, 0 V, 2.2 V); ◓ (magenta): (0 V, 1.83 V, 0 V, 1.73 V, 0 V); ◇ with + (dark yellow): (−23 V, 6.52 V, 5 V, 5 V, 5 V). (d) A low bias characteristic of the conductance (V_{sd} = 0.16 mV) for device D1 as a function of a top gate voltage V'_{t1} upon electrical gating V'_b = −23 V, V'_{t2} = V'_{t3} = V'_{t4} = 5 V at a base temperature. A series resistance of the RC filter, 22.4 kΩ, has been subtracted for all figures in the main text, except for Figure 3b,c,d and Figure 4a,b.

be modulated by a factor of 2. The minimum conductance has been observed at 0.145, 0.132, 0.140, and 0.180 e^2/h, respectively, associated with a Dirac point 4.0, 4.6, 2.4, and 2.2 V, for individually sweeping top-gate voltage V'_{t1}, V'_{t2}, V'_{t3}, and V'_{t4}. By performing a pair of top gates, for instance, V'_{t1} and V'_{t3}, the conductance can be further reduced to 0.119 e^2/h at a corresponding Dirac point with V'_{t1} = 1.83 V and V'_{t3} = 1.73 V. By further adjustments of top and back-gate voltages, the device conductance is eventually reduced to 0.104 e^2/h at a Dirac point with V'_b = −23 V, V'_{t1} = 6.52 V, V'_{t2} = V'_{t3} = V'_{t4} = 5 V, which is closed to a pinch-off. These measurements reveal that the top gate not only functions as a plunge gate but also modulates the barrier potential. Thus, the confinement barrier here is likely formed by inducing a band gap through the electrostatic gating together with local strain induced constriction. It is known that graphene could be deteriorated by the electron beam during the lithography process. The graphene deterioration could form barrier potentials underneath the top gates, which is a possible origin of the conductance suppression. Further investigation is needed to clarify the possibility of deterioration-induced conductance suppression in top-gated graphene QD devices.

A perpendicular electrical field breaks the layer inversion symmetry in FLG. Studies have observed that an external perpendicular electric field opens an energy gap tunable up to 250 meV in bilayer graphene.[22] Opening a band gap in r-TLG has been experimentally confirmed in the electrical transport measurement and optical spectroscopy.[23,24] As schematically shown in Figure 1a, we consider a QD device structure with the presence of a back gate and top gates, separated d_t and d_b from the top and bottom layer of r-TLG by a media of dielectric constant ε_r. The effective voltage between the gate and the closest graphene layer $V_{t,b} = V'_{t,b} - V^0_{t,b} = en_{t,b}d_{t,b}/\varepsilon_0\varepsilon_r$, which produces an electric field $E_{t,b} = en_{t,b}/\varepsilon_0\varepsilon_r$,[1,25,27] where $V'_{t,b}$ is the applied top/back gate voltage, $V^0_{t,b}$ is the effective offset voltage due to the initial environment induced carrier doping, ε_0 is the permittivity of the vacuum, and $n_{t,b}$ is the effective charge density on the top and the back gate. Upon electrical gating, the sum of effective charge between the top and back gate, $Q = \frac{\varepsilon_0\varepsilon_r V_b}{d_b} + \frac{\varepsilon_0\varepsilon_r V_t}{d_t} = en_b + en_t$, leads to a net carrier doping on graphene layers, resulting in a shift of the Fermi energy. Setting Q = 0 defines a charge neutral point (CNP) of graphene layers.[26] The difference of the two, $\delta Q = \frac{\varepsilon_0\varepsilon_r V_b}{d_b} - \frac{\varepsilon_0\varepsilon_r V_t}{d_t} = en_b - en_t$, breaks the inversion symmetry of graphene layers and generates a nonzero band gap.[26] By setting Q to zero and varying δQ, we can tune the Fermi level into the band gap to maintain zero carrier density in the top-gated regions while keeping a finite charge accumulation in the dot region due to an uncompensated back-gate voltage. In our experiment, the drain electrode is grounded. The Fermi energy and the band gap are tuned by top and back gate voltages (V'_t, V'_b). We have observed Coulomb oscillation patterns for these top-gated graphene QDs as varying the top/back gate voltage. Figure 3a shows Coulomb-blockade diamonds of the differential conductance for the device D1 as a function of bias voltage V_{sd} and a top gate voltage V'_{t1}. The voltages V'_b = −23 V, V'_{t2} = V'_{t3} = V'_{t4} = 5 V are held constant. The charging energy extracted from the measurement is about $E_c \sim 0.32$ meV, corresponding to a dot capacitance, $C \sim 500$ aF. The addition energy ranges from 46.7 to 93.3 meV. Thus, the lever arm for conversion of gate voltages into energies is estimated to be 0.34% ∼ 0.69%. A low bias characteristic of the conductance (V_{sd} = 0.16 mV) for device D1 is plotted as a function of a top gate voltage V'_{t1} upon electrical gating V'_b = −23 V, V'_{t2} = V'_{t3} = V'_{t4} = 5 V, as shown in Figure 2d. The transport is tuned from the electron (left-hand side) to the hole regime. The conductance is strongly suppressed within the transition region 5.86 V < V'_{t1} < 6.83 V, indicated by two arrows. This conductance-suppressed region is so-called "transport gap". A sequence of reproducible resonances is revealed in the transport gap, which are corresponding to the Coulomb diamonds shown in Figure 3a. The transport gap is measured at a constant V_{sd} (nearly zero), but varying Fermi energy E_F. Following the method used in the report,[36] we estimate the energy scale of "transport gap", $\Delta E_F = \hbar\Delta k \cdot v_F = \hbar v_F\sqrt{2\pi c_g \Delta V'_t/|e|} \sim 50.3$ meV, according to our simulated top-gate capacitance, where c_g is the gate capacitance per area and $v_F \sim 10^6$ ms^{-1} is the Fermi velocity of charge carriers. It is worthy to note that this formula is derived based on the characteristic linearly dispersing band of single-layer graphene. Considering the nonlinear dispersion of "Mexican hat" shaped low-energy band in r-TLG for our device, the "transport gap" should be corrected to count for the

DOI: 10.1021/acs.nanolett.6b02522
Nano Lett. XXXX, XXX, XXX−XXX

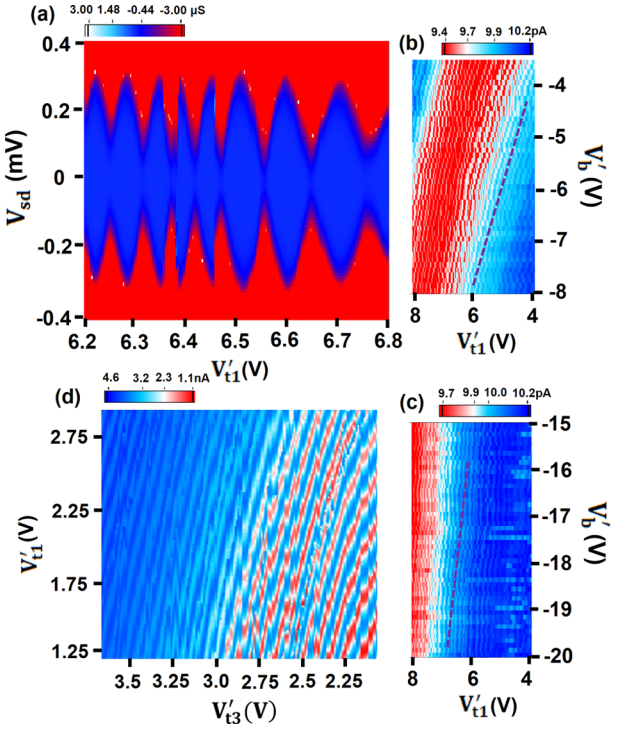

Figure 3. (a) Coulomb-blockade diamonds of the differential conductance as a function of bias voltage V_{sd} and a top gate voltage V'_{t1} at a base temperature. The voltages $V'_b = -23$ V, $V'_{t2} = V'_{t3} = V'_{t4} = 5$ V are held constant. (b) and (c) Coulomb resonances as a function of the back and top gate voltage at a fixed source−drain voltage $V_{sd} = 1$ mV, and $V'_{t2} = V'_{t3} = V'_{t4} = 0$ V at a base temperature. The slope of dashed lines gives a relative lever arm of top/back gate to be $\alpha^t_b \sim 2.04$ and 4.85 in a region of back gate voltage -8 V $< V'_b < -3.5$ V (b) and -20 V $< V'_b < -15$ V (c), respectively. (d) A low-bias conductance measurement as a function of the V'_{t1} and V'_{t3} with $V_{sd} = 0.5$ mV and $V'_b = V'_{t2} = V'_{t4} = 0$ V at a base temperature.

quadratic dispersion. Thus, it could be roughly estimated to be $\Delta E_F = \frac{p^2 v_F^2}{\gamma_1} = \frac{\hbar^2 \Delta k^2 v_F^2}{\gamma_1} \sim 9.0$ meV, where $\gamma_1 = 0.38$ eV. As discussed below, a band gap opening of 4.0 meV is estimated due to the electrical gating. Thus, the local strain induced barrier could have contributed more than half of total constriction barriers.

Figure 3b shows a low-bias conductance measurement as a function of the V'_b and V'_{t1} at a fixed source−drain voltage $V_{sd} = 1$ mV. A sequence of essentially straight tilted lines has been observed implying Coulomb blockade resonances of the QD. The corresponding relative lever arm of top/back gate is given by $\alpha_{t/b} \sim 2.04$ in the region of low negative back gate voltage -8.0 V $< V_g < -3.5$V. The slope of tilted lines changes abruptly as the back gate voltage further decreases. The relative lever arm turns to be $\alpha_{t/b} \sim 4.85$ in the region -20 V $< V_g < -15$ V, as shown in Figure 3c. This reduction of the relative lever arm reflects a weakening of gating effect at large negative back gate voltage. Although highly doped Si substrate was used for the global back gate, the conductivity of the substrate was significantly reduced at the base temperature due to the freezing out of the carriers in the substrate. The effective offset voltage V^0_b and V^0_t, due to the initial environment induced carrier doping, can be extracted by the zero-bandgap CNP ($Q = 0$, $\delta Q = 0$), to be $V^0_b \sim -6.6$ V and $V^0_t \sim 1.6$ V in the region of large negative back gate voltage. Upon electrical gating $V'_t = 5$ V and $V'_b = -23$ V, the Fermi level could be tuned into the band gap in the top-gated regions, while holes accumulated in the dot region. Extending top gate voltage further positive cannot push the QD into a single-electron regime, so it is impossible to absolutely determine the number of holes in the dot. Figure 3d shows a low-bias conductance measurement as a function of the V'_{t1} and V'_{t3} with $V_{sd} = 0.5$ mV. The observed straight tilted lines imply Coulomb blockade resonances. The conductance measurements have revealed the modulation of barrier potentials by the top gate voltage, which should lead to a change in the QD size and charging energy as varying the gate voltage. Indeed, we have observed a modulation of the QD addition energy with changing a gate voltage. Figure S2c and d in the Supporting Information shows a monotonic change of the addition energy as a function of the top gate V'_{t1} and V'_{t3}, respectively. The addition energy varies by changing the back-gate voltage as well, as shown in Figure S3b.

To obtain a better quantitative understanding of the gate-defined QD, we use a commercial finite element analysis simulation tool (COMSOL) to calculate the barrier potential and band structure of a top gate-defined QD in r-TLG. The induced charges on the different graphene layers, n_1, n_2, and n_3, can be determined by the $V_{t,b}$ via the relation $n_t + n_b + \sum_{i=1}^{3} n_i = 0$. Considering a uniform electric field $E_i = en_i/\varepsilon_0\varepsilon_r$, the layer asymmetries between the first and second layers, as well as between the second and third layers are determined by a corresponding change in the potential energy $\Delta_{1,2}$ and $\Delta_{2,3}$, $\Delta_{1,2} = (n_2 + n_3 + n_b)e^2c_0/\varepsilon_0\varepsilon_r$, $\Delta_{2,3} = (n_3 + n_b)e^2c_0/\varepsilon_0\varepsilon_r$, which break the inversion symmetry of graphene and generate a nonzero band gap,[25,27] where $c_0 = 0.35$ nm is the interlayer distance. By using a self-consistent Hartree approximation to calculate the induced charges on the different graphene layers, we simulated the barrier potential and band structure of a trilayer graphene system in the presence of the top and back gates. The simulation method was discussed in more detail in the Supporting Information. Figure 1c shows a low-energy band structure of r-TLG around the K point in the region beneath the top gate, upon electrical gating $V'_t = 5.0$ V and $V'_b = -22.6$ V to match the experimental condition. The band structure consists of a set of six cubic bands with four of them crossing at an energy $E = \gamma_1 \sim 0.38$ eV above (below) the K point,[27] consistent with the previous theoretical calculation.[9] For the other two lower energy bands, a band gap of about 4.0 mV is feasible in the zoomed area (Figure 1d), under the corresponding asymmetric potentials $\Delta_{1,2}/e \sim 3.94$ mV and $\Delta_{2,3}/e \sim 4.05$ mV from the self-consistent calculation. According to the top-gate geometry and electrostatic gating of the QD device, we calculated the profile of barrier potentials (Figure 1e), conduction and valence band (Figure S4 in Supporting Information). The dot size (diameter) is estimated to be $d_{dot} \sim 500$ nm, from the area bounded by the closed portion of the contour line at the saddle points of the barrier potential in Figure 1e, consistent with the lithographic dimension of QD. A maximum height of the potential barrier ~9 mV was obtained for the gate-defined constriction. The band gap opening due to the local strain was not included in our calculation. Further investigation may deem desirable to explore the potential application of strain engineering by exploiting different device geometries and different thermal coefficients of gate and insulating materials.

The mass term generated by the layer asymmetry breaks the inversion symmetry between graphene layers, while the perpendicular magnetic field breaks the effective time-reversal

DOI: 10.1021/acs.nanolett.6b02522
Nano Lett. XXXX, XXX, XXX−XXX

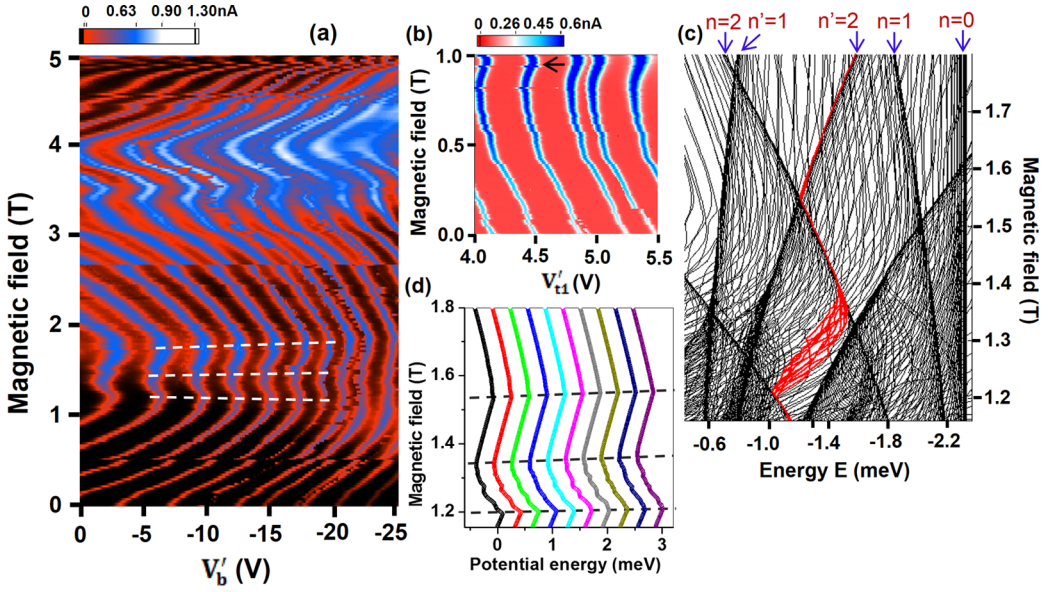

Figure 4. (a) Evolution of Coulomb resonances in device D1 as a function of the back gate voltage and magnetic field perpendicular to the graphene plane at a base temperature. The voltages V_{sd} = 0.1 mV, V'_{t1} = 5.75 V, V'_{t2} = 5.9 V, V'_{t3} = 5.0 V, V'_{t4} = 4.85V are held constant. The dashed lines indicate the kinks where the trend of energy spectra changes the direction. (b) Coulomb resonances in device D1 as a function of the top gate voltage V'_{t1} and the perpendicular magnetic field at a base temperature. The voltages V_{sd} = 0.1 mV, V'_b = −23, V'_{t2} = 5.9 V, V'_{t3} = 5.0 V, V'_{t4} = 4.85 V are held constant. (c) A simulation of the low energy-level spectrum as a function of the perpendicular magnetic field for device D1, upon electrical gating V'_t = 5.0 V and V'_b = −22.6 V. (d) 10 converged energy levels indicated by the red lines in (c) are chosen and converted into electrochemical potential energies by adding a charging energy of 0.32 meV. For clarity, the electrochemical potential for the first energy level (black curve) is set to zero at B = 1.15 T.

symmetry.[14,28] Thus, the combination of a mass-term and magnetic field breaks all the orbital degeneracies. The magnetic field dependence of energy levels has been theoretically investigated in gapped single- and bilayer QDs.[14,29] The results show that the valley degeneracy is broken by a magnetic field applied perpendicular to the graphene plane. Several recent theoretical studies have focused on the Landau level spectrum of ABA- and ABC-stacked trilayer graphene.[8−10] Numerical simulations reveal that six cubic bands of ABC TLG lead to three groups of Landau levels (LLs) with intergroup and intragroup LL anticrossings.[9] Instead of focusing on the graphene sheet, we exploited the evolution of Coulomb resonances with a magnetic field B in top-gated QD devices. In Figure 4a, we show the Coulomb resonances in device D1 as a function of a back gate voltage and a magnetic field perpendicular to the graphene plane. A small bias voltage of 0.1 mV applied to the device allows probing the magnetic field dependence of exquisite detailed energy-level spectra in QD. Experimental data shows current peaks displaying a unique complex evolution as increasing the magnetic field B. The energy level first shifts toward a high energy (negative back gate voltage), following a kink as B reaches about 1.22 T, and then turns in a contrary direction toward a low energy. A second kink appears when $B \sim 1.36$ T, where the trend of energy spectra changes the direction again and presents a third kink at $B \sim 1.59$ T. The dashed lines in the figure indicate the pronounced kinks where the trend of energy spectra changes the direction. These kinks may be attributed to the intragroup LL crossings of energy spectrum. Since the data were taken in 2 days, there is no surprise that an abrupt shift of oscillation patterns occurs when B = 0.50 T and 2.66 T, probably due to the disturbed potential shift from charge traps in the insulator layer. Kink features are also found in Coulomb resonances as a function of the top gate voltage at a magnetic field of about 0.97 T, as shown in Figure 4b. Similar kink features have been observed in the energy level spectrum of the monolayer graphene QD.[5,6,30−32]

To elucidate the evolution of Coulomb oscillations, we performed numerical calculations for the eigenenergies of a r-TLG QD in the presence of a perpendicular magnetic field (see Supporting Information for details). We calculated the magnetic field dependence of energy-level spectrum in a r-TLG QD. The result shows three groups of Landau levels, with one set of LLs starting from zero energy and two sets of LLs at an energy γ_1, which correspond to the low-energy band that touches the Dirac point and those cross at γ_1, respectively (see Figure 1c). Figure 4c shows a zoomed area of the calculated low-energy spectrum for QD device D1, as a function of the magnetic field upon electrical gating V'_t = 5.0 V and V'_b = −22.6 V. In our case, the magnetic length, $l_B = \sqrt{\frac{\hbar}{eB}}$, is smaller than the dot size; thus we expect the density of states to converge toward Landau levels. We indeed observed some characteristics of low-energy Landau levels labeled $n(n')$ = 0−3 in the figure, for two branches which bend upward and downward, respectively. Landau levels in different branches feature a kink at the level crossing. These level crossings reflect the hybridized nature of energy-level spectrum of TLG QD. Our transport measurement is a direct measure of electrochemical potential $\mu_{dot}(N)$ in the bias window V_{sd}; thus, the calculated single-particle energy E_n needs to be mapped into an electrochemical potential $\mu_{dot}(N)$ for comparison, by a relation $\mu_{dot}(N) \sim E_n + E_c$, where E_c is the charging energy of the QD and N is the number of electrons/holes in the dot.[33] In consequence, we chose 10 converged energy levels from the Landau levels indicated by the red lines in Figure 4c,[34] and converted them into electrochemical potentials, plotting in Figure 4d by adding a charging energy of 0.32 meV. For clarity, the electrochemical

DOI: 10.1021/acs.nanolett.6b02522
Nano Lett. XXXX, XXX, XXX−XXX

potential for the first energy level (black curve) is set to zero at B = 1.15 T. Three series of kinks are indicated by dashed lines in the figure, positioned at $B \sim$ 1.21 T, 1.36 T, and 1.58 T, respectively, which are well matching the experimental observation of kink locations at 1.22 T, 1.36 T, and 1.59 T (see the corresponding dashed lines in Figure 4a). Moreover, the overall trend of the simulated magnetic field dependence is consistent with experimental observations, implying the hybridized energy-level spectrum of QD in FLG.

To define spin qubits in graphene QDs, a valley splitting must be larger than Zeeman splitting so that only the lower spin levels have to be considered. Considering a perpendicular magnetic field B = 3 T, we obtain a Zeeman splitting $g\mu_B B \approx$ 0.35 meV with a g factor $g \sim 2$,[6] where μ_B is the Bohr magneton. A valley splitting is estimated to be $\tau\mu_B^* B$, where τ refers to the valley index ($\tau = \pm 1$). The effective magnetic moment $\mu_B^* \sim \frac{m_0}{m^*}\left(\frac{2p^2}{p_0^2} - 1\right)\mu_B$,[35] where m_0 is the mass of free electron, $m^* \sim 0.012m_0$ is the effective electron mass in bilayer graphene, p (p_0) is the electron momentum.[8] At a band gap minimum $p = p_0$, the valley splitting is about 28.9 meV, which is much larger than the Zeeman splitting. These results suggest that such QDs confined in FLG graphene could be an ideal host for spin qubits.

In summary, we have investigated the functionality of top-gate defined QDs in FLG. We observed a suppression of device conductance at a low temperature even without the application of external gate voltages. We ascribe these observations to the induced local strain by a mismatch in thermal expansion coefficients of gate metal, insulating layer, and substrate. Local strains alone could not pinch off the conductance completely; thus to define a dot constriction, a perpendicular electrical field is required to further enhance tunnel barriers beneath the top gates. Our transport measurements unambiguously reveal that confinement barriers are formed by inducing a band gap via the electrostatic gating together with local strain induced constrictions. The investigation in energy-level spectra reveals a complex evolution of Coulomb oscillations with a perpendicular magnetic field, featuring kinks at level crossings. The numerical calculation confirms the band gap opening by a perpendicular electric field in FLG QD. The simulation of energy spectrum shows that kink features and overall trend of the magnetic field dependence are consistent with the experimental observation. Potential application of this electrostatic gating and strain engineering would be desirable to confine QDs in FLG for spin qubits.

■ ASSOCIATED CONTENT

Supporting Information

The Supporting Information is available free of charge on the ACS Publications website at DOI: 10.1021/acs.nanolett.6b02522.

Description of the measured devices; AFM image; Raman spectroscopy; gate voltage dependence of resonance peak spacing; band structure simulations; simulations for the magnetic field dependence of energy-level spectrum (PDF)

■ AUTHOR INFORMATION

Corresponding Authors

*E-mail: lmduan@umich.edu.

*E-mail: ypsong@mail.tsinghua.edu.cn.

Notes

The authors declare no competing financial interest.

■ ACKNOWLEDGMENTS

We thank Chengyao Li for the technical support. This work was supported by the Ministry of Education of China through its grant to Tsinghua University and the National Natural Science Foundation of China under Grant No. 11474177.

■ REFERENCES

(1) McCann, E.; Koshino, M. *Rep. Prog. Phys.* **2013**, *76*, 056503.

(2) Castro Neto, A. H.; Guinea, F.; Peres, N. M. R.; Novoselov, K. S.; Geim, A. K. *Rev. Mod. Phys.* **2009**, *81*, 109.

(3) Fischer, J.; Trauzettel, B.; Loss, D. *Phys. Rev. B: Condens. Matter Mater. Phys.* **2009**, *80*, 155401.

(4) Coish, W. A.; Loss, D. *Phys. Rev. B: Condens. Matter Mater. Phys.* **2004**, *70*, 195340.

(5) Güttinger, J.; Stampfer, C.; Libisch, F.; Frey, T.; Burgdörfer, J.; Ihn, T.; Ensslin, K. *Phys. Rev. Lett.* **2009**, *103*, 046810.

(6) Güttinger, J.; Frey, T.; Stampfer, C.; Ihn, T.; Ensslin, K. *Phys. Rev. Lett.* **2010**, *105*, 116801.

(7) Liu, X. L.; Hug, D.; Vandersypen, L. M. K. *Nano Lett.* **2010**, *10*, 1623.

(8) Tang, K. C.; Qin, R.; Zhou, J.; Qu, H.; Zheng, J.; Fei, R.; Li, H.; Zheng, Q.; Gao, Z.; Lu, J. *J. Phys. Chem. C* **2011**, *115*, 9458.

(9) Yuan, S. J.; Roldán, R.; Katsnelson, M. I. *Phys. Rev. B: Condens. Matter Mater. Phys.* **2011**, *84*, 125455.

(10) Sena, S. H. R.; Pereira, J. M.; Peeters, F. M.; Farias, G. A. *Phys. Rev. B: Condens. Matter Mater. Phys.* **2011**, *84*, 205448.

(11) Allen, M. T.; Martin, J.; Yacoby, A. *Nat. Commun.* **2012**, *3*, 934.

(12) Taychatanapat, T.; Jarillo-Herrero, P. *Phys. Rev. Lett.* **2010**, *105* (16), 166601.

(13) Müller, A.; Kaestner, B.; Hohls, F.; Weimann, T.; Pierz, K.; Schumacher, H. W. *J. Appl. Phys.* **2014**, *115*, 233710.

(14) Recher, P.; Nilsson, J.; Burkard, G.; Trauzettel, B. *Phys. Rev. B: Condens. Matter Mater. Phys.* **2009**, *79*, 085407.

(15) Trauzettel, B.; Bulaev, D. V.; Loss, D.; Burkard, G. *Nat. Phys.* **2007**, *3*, 192.

(16) Lui, C. H.; Li, Z.; Chen, Z.; Klimov, P. V.; Brus, L. E.; Heinz, T. F. *Nano Lett.* **2011**, *11*, 164.

(17) Li, H.; Wu, J.; Huang, X.; Lu, G.; Yang, J.; Lu, X.; Xiong, Q.; Zhang, H. *ACS Nano* **2013**, *7*, 10344.

(18) Hao, Y. F.; Wang, Y. Y.; Wang, L.; Ni, Z. H.; Wang, Z.; Wang, R.; Koo, C. K.; Shen, Z.; Thong, J. T. L. *Small* **2010**, *6*, 195.

(19) Jhang, S. H.; Craciun, M. F.; Schmidmeier, S.; Tokumitsu, S.; Russo, S.; Yamamoto, M.; Skourski, Y.; Wosnitza, J.; Tarucha, S.; Eroms, J.; Strunk, C. *Phys. Rev. B: Condens. Matter Mater. Phys.* **2011**, *84*, 161408R.

(20) Choi, S.-M.; Jhi, S.-H.; Son, Y.-W. *Nano Lett.* **2010**, *10*, 3486.

(21) Pereira, V. M.; Castro Neto, A. H. *Phys. Rev. Lett.* **2009**, *103*, 046801.

(22) Castro, E. V.; Novoselov, K. S.; Morozov, S. V.; Peres, N. M. R.; dos Santos, J. M. B. L.; Nilsson, J.; Guinea, F.; Geim, A. K.; Neto, A. H. C. *Phys. Rev. Lett.* **2007**, *99*, 216802.

(23) Lui, C. H.; Li, Z.; Mak, K. F.; Cappelluti, E.; Heinz, T. F. *Nat. Phys.* **2011**, *7*, 944.

(24) Khodkov, T.; Khrapach, I.; Craciun, M. F.; Russo, S. *Nano Lett.* **2015**, *15*, 4429.

(25) Avetisyan, A. A.; Partoens, B.; Peeters, F. M. *Phys. Rev. B: Condens. Matter Mater. Phys.* **2010**, *81*, 115432.

(26) Zhang, Y.; Tang, T.-T.; Girit, C.; Hao, Z.; Martin, M. C.; Zettl, A.; Crommie, M. F.; Shen, Y. R.; Wang, F. *Nature* **2009**, *459*, 820.

(27) Avetisyan, A. A.; Partoens, B.; Peeters, F. M. *Phys. Rev. B: Condens. Matter Mater. Phys.* **2009**, *80*, 195401.

(28) Recher, P.; Trauzettel, B. *Nanotechnology* **2010**, *21*, 302001.

(29) Zarenia, M.; Partoens, B.; Chakraborty, T.; Peeters, F. M. *Phys. Rev. B: Condens. Matter Mater. Phys.* **2013**, *88*, 245432.

DOI: 10.1021/acs.nanolett.6b02522
Nano Lett. XXXX, XXX, XXX−XXX

(30) Schnez, S.; Ensslin, K.; Sigrist, M.; Ihn, T. *Phys. Rev. B: Condens. Matter Mater. Phys.* **2008**, *78*, 195427.
(31) Lin, Y.-P.; Wang, J.; Lu, J.-M.; Lin, C.-Y.; Lin, M.-F. *RSC Adv.* **2014**, *4*, 56552.
(32) Güttinger, J.; Stampfer, C.; Frey, T.; Ihn, T.; Ensslin, K. *Nanoscale Res. Lett.* **2011**, *6*, 253.
(33) Kouwenhoven, L. P.; Austing, D. G.; Tarucha, S. *Rep. Prog. Phys.* **2001**, *64*, 701.
(34) Ashoori, R. C.; Stormer, H. L.; Weiner, J. S.; Pfeiffer, L. N.; Baldwin, K. W.; West, K. W. *Phys. Rev. Lett.* **1993**, *71*, 613.
(35) Koshino, M.; Ando, T. Electronic Properties of Monolayer and Multilayer Graphene. In *Physics of Graphene*; Aoki, H., S. Dresselhaus, M., Eds.; Springer International Publishing: Cham, 2014; pp 173−211.
(36) Stampfer, C.; Güttinger, J.; Hellmüller, S.; Molitor, F.; Ensslin, K.; Ihn, T. *Phys. Rev. Lett.* **2009**, *102*, 056403.

DOI: 10.1021/acs.nanolett.6b02522
Nano Lett. XXXX, XXX, XXX−XXX